ChemComm

COMMUNICATION

View Article Online
View Journal | View Issue

Cite this: *Chem. Commun.*, 2017, 53, 2499

Received 7th January 2017,
Accepted 25th January 2017

DOI: 10.1039/c7cc00140a

rsc.li/chemcomm

Insight into the enhanced photoelectrocatalytic activity in reduced $LaFeO_3$ films†

Yu Sun, Xiaofeng Wu, Long Yuan, Meng Wang, Mei Han, Liqun Luo, Beining Zheng, Keke Huang and Shouhua Feng*

$LaFeO_3$ films, as photoelectrocatalysts, could be slightly reduced by annealing in an oxygen-deficient atmosphere. The introduced oxygen vacancies increase the electrical conductivity and change their surface band structures which endows $LaFeO_3$ films with a higher oxygen evolution reaction current and a lower overpotential.

Photoelectrocatalytic splitting of water into hydrogen and oxygen, as a promising method for solar energy conversion into a clean and renewable source, has always been a focus of scientific research.[1] However, the half-reaction of the oxygen evolution reaction[2] (OER) is much more difficult than the half-reaction of the hydrogen evolution reaction,[3] which limits the application of water splitting. This is because OER consists of several steps with large reaction barriers, which require large overpotentials to drive the reaction at suitable rates. Large overpotentials always induce huge efficiency losses and limit the practicability of water splitting. An ideal OER catalyst[4] should possess a suitable band gap, good stability, economic chemical components and high energy conversion efficiency. Although good catalytic activity[5] has been achieved by IrO_2 and RuO_2, efforts are ongoing to develop OER catalysts based on considerably cheaper metal oxides.

The flexible crystal structure of ABO_3 endows perovskite oxides with unique photo-response and excellent carrier mobility. And their intrinsic activity[6] is comparable to the best and most stable catalysts such as IrO_2 and RuO_2. In particular, Fe based perovskite oxides possess the potential to be highly active catalysts for OER because of their visible range band gap. Exposure of more active sites has been used to improve their catalytic activity by increasing the specific surface area.[7] And precise element doping makes it possible to improve the catalytic performance of the material itself.[8] However, the OER kinetics has not been changed and is still sluggish.

State Key Laboratory of Inorganic Synthesis and Preparative Chemistry, College of Chemistry, Jilin University, Changchun 130012, P. R. China. E-mail: shfeng@mail.jlu.edu.cn

† Electronic supplementary information (ESI) available: Detailed experimental section, XRD for LFO powders and rocking curves, SEM, UV-Vis absorption spectrum and EIS for LFO films are included. See DOI: 10.1039/c7cc00140a

Through modification of surface–oxygen interaction, oxygen vacancies could greatly reduce the kinetic barrier.[9] Meanwhile, due to vacancy-induced electron doping,[10] the increased electrical conductivity shows high photon to current conversion efficiency. Herein, oxygen vacancies are introduced into $LaFeO_3$ films by *in situ* annealing in an oxygen-deficient atmosphere using Pulsed Laser Deposition (PLD). A detailed experimental section can be found in the ESI.† By characterizing the films using X-ray photoelectron spectroscopy (XPS), electron spin resonance (ESR) spectroscopy, photoluminescence (PL) spectroscopy, ultraviolet-visible (UV-Vis) absorption spectroscopy, scanning electron microscopy (SEM), high-resolution X-ray diffraction (XRD), electrochemical impedance spectroscopy (EIS) and linear sweep voltammetry (LSV), their crystal and band structures are effectively related to the OER performance.

Binding energies of the Fe 2p core level for LFO films annealed under different oxygen pressures are shown in Fig. 1(a) and the carbon 1s peak at 284.8 eV is used to calibrate the energy scale. All main peaks of Fe $2p_{3/2}$ locate at 710.5 eV, indicating that the iron in LFO films primarily presents in the Fe^{3+} oxidation state. With lowering of the annealing oxygen pressure, slight broadening of the main peak on the low binding energy side becomes distinct. In particular for films annealed under 4×10^{-2} and 4×10^{-4} Torr oxygen pressures, obvious shoulder peaks[11] at 709.2 eV appear. They may arise from the slight reduction of some Fe^{3+} to Fe^{2+}. Simultaneously, the increased peak intensity of the satellite peak[12] for Fe^{2+} at 713 eV also becomes more distinct. Thus, in chemical formula $LaFeO_{3-x}$, the higher oxygen vacancy concentration makes more ratio of Fe^{2+} to maintain the electric neutrality. It has been reported that some of Fe^{3+} were reduced to Fe^{2+} under high-temperature calcination.[13] With a similar treatment, Flynn *et al.* even found Fe^0 on the LFO surface[14] by angle-resolved XPS with escape electrons taking off at angles of 10°. While Fe^0 was not directly detected by our limited ordinary XPS system, the gradually increasing conductivity (discussed in the next paragraph) strongly indicates the formation of a metallic phase (in Fig. 1(b)). It may come from the Fe^0 in the metal state which is in common with their work. And a similar situation has also been reported by

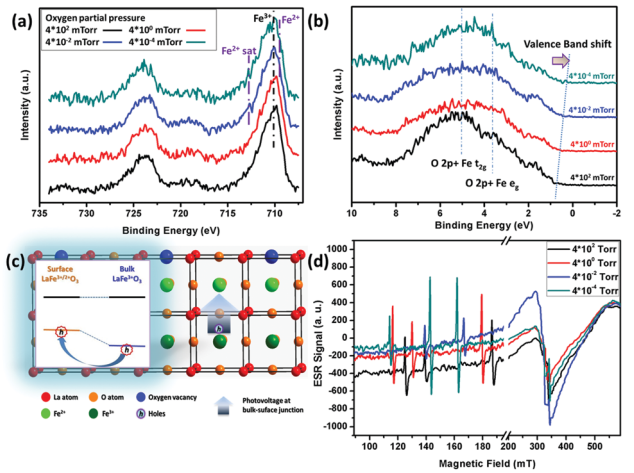

Fig. 1 Characterization of LFO films annealed under different oxygen pressures. (a) Binding energy of Fe 2p. (b) Normalized valence band spectra. (c) Band structure of the bulk–surface heterojunction. (d) Electron paramagnetic resonance spectra.

others using the valence band spectra.[15] Alternatively, the amount of near-surface Fe^0 is inaccessible for XPS measurements for the core level of Fe^0. It has been confirmed that the formation of Fe^0 on the $La_{0.6}Sr_{0.4}FeO_3$ (LSF) surface, induced by cathodic polarization,[16] showed a great improvement in the electrochemical water splitting activity of the electrodes. Through the investigation of changes in surface chemistry and water splitting kinetics of the perovskite-type mixed conductor LSF, Opitz *et al.* suggested a fundamental difference in the water-splitting mechanism on LSF with and without Fe^0.

The valence band structure near the Fermi Level is the key factor to the OER. So valence band spectra of LFO films annealed under different oxygen pressures are collected in Fig. 1(b). With increasing the oxygen vacancy concentration, the top of valence bands shift (shown as the dotted line in Fig. 1b) toward the Fermi Level, indicating that the electrical conductivity increases gradually.[17] Naturally, this will lead to a high photon to current conversion efficiency, and the catalytic performance for OER is thus improved correspondingly. It is also experimentally confirmed by the smaller impedance in electrochemical impedance spectroscopy measurements (in the ESI†). The increased electrical conductivity may come from the following two aspects. On the one hand, oxygen vacancies, acting as donors, will lead to electron doping. On the other hand, carrier transfer in perovskites is restricted by two exchange mechanisms: superexchange and double exchange. In superexchange,[18] the electrons do not actually move between the adjacent Fe^{3+}. In double exchange,[19] the electrons are itinerant, *i.e.* they actually move between Fe^{3+} and Fe^{2+} *via* the intermediate ligand oxygen; this results in the material displaying magnetic exchange coupling as well as metallic conductivity.

In addition, the presence of Fe^{2+} is also correlated with the increased density of states near the Fermi level in the valence band spectra and the component of the top valence band also changes obviously. It mainly consists of (O 2p + Fe t_{2g}) and (O 2p + Fe e_g) hybrid orbitals,[20] at 5.0 eV and 3.8 eV respectively. More oxygen vacancies increase the ratio of (O 2p + Fe e_g) hybrid orbitals. Shao-Horn *et al.* have proved that greater hybridization between B-site and oxygen promotes the charge transfer between surface cations and adsorbates such as O_2^{2-} and O^{2-} in the rate-determining steps of OER, which can result in a higher OER activity.[6]

Furthermore, annealing in vacuum could change the chemical structure only on the surface. The gradually changed (from bulk to surface) defect chemistry, in a sense, leads to a continuous change in the band structure. Consequently, the formation of a bulk–surface heterojunction (bulk: $LaFe^{3+}O_3$; surface: $LaFe^{3+/2+}O_{3-x}$) (Fig. 1(c)), resulted from the valence band offset (Fig. 1(b)), will promote the separation of photon-generated carriers and accelerate the collection of holes on films' surface. The development of photovoltage at the bulk–surface heterojunction will endow holes with additional potential to accelerate the OER kinetic process and decrease the overpotential.

Oxygen vacancies are confirmed by ESR in Fig. 1(d). All films are composed of an asymmetric pattern at a magnetic field of 200–500 mT. This can be attributed to the different valence states of Fe. The decrease in annealing pressure will increase the asymmetry,[21] namely the proportion of Fe^{2+}. Resonance signals at a lower magnetic field of 100–200 mT may come from the defect complexes[22] between the oxygen vacancy (V_O) and acceptor centres, such as Fe^{3+}–V_O and Fe^{2+}–V_O. The relative intensity of resonance signals from defect complexes (compared with the intensity of asymmetric patterns) could be used to qualitatively compare the concentration of oxygen vacancies. As predicted, LFO films annealed under an oxygen pressure of 4×10^{-4} Torr possess the largest concentration of oxygen vacancies. These signal shifts about the magnetic field may come from the change in the crystal structure.

In perovskites (ABO_3), photoexcited carriers (photocurrent) transfer through the B–O–B atom chains. The crystal structures of LFO films are studied by high-resolution XRD as shown in Fig. 2(a). According to Bragg's equation: $\lambda = 2d \sin\theta$, the lattice constant (interplanar spacing of LFO (004)) becomes larger with the decrease in oxygen pressure. Considering the electronegativity and electrostatic potential, the bond length of Fe^{2+}–O is longer than that of Fe^{3+}–O and the ion radius of Fe^{2+} is relatively smaller in the same coordination environment. So a higher concentration of Fe^{2+} will macroscopically display a larger lattice constant. According to literature studies, oxygen vacancies near the surface could enhance the catalytic efficiency because of the increased number of active sites around these defects. Here, lattice expansion is beneficial for exposing more active sites.

As good candidates for p-type photocathode materials, Fe based perovskite oxides show a good photoresponse to visible light due to their suitable band gaps.[23] Here, optical absorbance spectra (in the ESI†) are used to study the relationship between band gap and annealing oxygen pressure. The band gaps can be estimated from the tangent lines in the plots of the square root of the Kubelka–Munk functions against the photon energy: $\alpha h\nu = A(h\nu - E_g)^n$, as shown in Fig. 2(b). With increasing oxygen vacancy concentration, the band gaps decrease gradually from 2.47 eV, 2.42 eV, 2.40 eV to 2.37 eV. This is because lattice expansion will delocalize electrons from the crystal lattice and induce a smaller band gap.[24] (In extreme cases, when the lattice

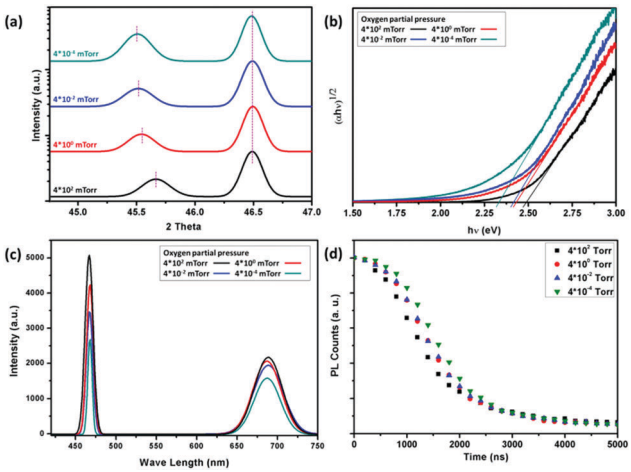

Fig. 2 (a) High-resolution XRD patterns for LFO films annealed under different oxygen pressures with unchanged substrates STO (002). The slight down-shift of the epi-peaks of LFO (004) means lattice expansion. (b) Optical absorbance spectra have been converted into the form of the Kubelka–Munk function to show the absorption edge shift. (c) Photoluminescence spectra with an excitation wavelength of 290 nm. (d) Photoluminescence lifetime at an emission wavelength of 466 nm.

constant is infinitely large, atoms do not show any constraint to outer electrons. All of outer electrons could be regarded as free electrons and the band gap is 0.) A smaller band gap means a wider solar spectra response and more energy can be captured. The catalytic performance for OER (photocurrent) will be promoted by increasing the concentration of photoexcited carriers.

For better understanding the presence of defects in the samples, we used a combined fluorescence lifetime and steady state spectrometer to investigate the room temperature photoluminescence spectra of LFO films. In Fig. 2(c), we find that all the $LaFeO_3$ films exhibit two obvious PL peaks at about 466 and 687 nm. With decreasing annealing oxygen pressure, the PL emission intensities decrease. It is known that PL emission is a result of the recombination of photoexcited electrons and holes. A lower emission intensity of luminescence indicates a lower recombination rate which results in a better photocatalytic performance. This can also be confirmed by the increased photoluminescence lifetime (Fig. 2(d)). It could be attributed to the charge transfer at the bulk–surface junction.

Linear sweep voltammetry is used to estimate the catalytic performance for OER on LFO film electrodes. Due to OER kinetic losses at the film–electrolyte junction, all LFO film electrodes present large overpotentials (Fig. 3). OER dark current gradually increases with the oxygen vacancy concentration. After excluding the effects of surface topography and crystalline quality using SEM and XRD (ESI†), it mainly results from the following two aspects. Firstly, the increase in electrical conductivity will reduce the possibility for carriers to be scattered by impurities. Secondly, surface Fe^{3+} is reduced to Fe^{2+} (maybe some atomic species Fe^0). Chemically driven formation of metal particles from perovskite materials under reducing conditions or nonstoichiometric ratios[25] has been used to enhance electrochemical kinetics. Changing the ratio of Fe^{3+}/Fe^{2+} will accelerate holes' transfer process for OER and offer a faster

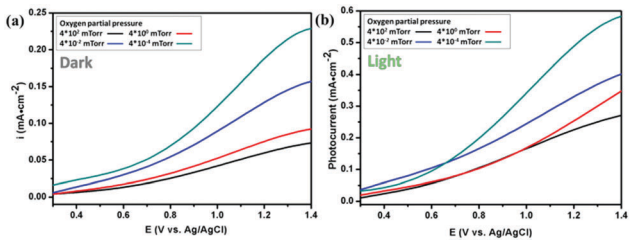

Fig. 3 (a) Dark current, (b) photocurrent of OER in 0.1 M KOH for LFO films annealed under different oxygen pressures.

electrode kinetics.[26] And a promoted electrochemical kinetics by two phases (a metal and an oxide phase) has been reported for perovskite-type electrodes.[25] Irradiation with a 300 W Xe arc lamp leads to a negative shift for the onset voltage of OER and a considerable increase in the OER current (Fig. 3(b)). The negative voltage shift may result from the additional overpotential provided by the photovoltage at the bulk–surface junction. The increase in the OER current can be attributed to more photon-generated carriers and their longer lifetime.

In summary, annealing of LFO films in an oxygen-deficient atmosphere has been used to promote their catalytic performance for OER. Due to the introduction of oxygen vacancies, improvement in electrical conductivity on the surface increases the OER current. At the same time, greater hybridization between the B-site and oxygen promotes charge transfer between surface cations and adsorbates. In addition, a longer bond length of Fe–O results in a larger lattice constant which means a weaker constraint to carriers. It will also give rise to a narrowing of the optical band gap, and more energy can be harvested to promote the photocurrent for OER. Furthermore, the valence band shift toward the Fermi level (valence band offset) leads to the formation of a bulk–surface junction (bulk: $LaFe^{3+}O_3$; surface: $LaFe^{3+/2+}O_{3-x}$) and it effectively reduces the overpotential for OER photoelectrocatalysis.

This work was supported by the National Natural Science Foundation of China (grants 21131002, 21427802, and 21671076).

Notes and references

1 H. B. Wu, B. Y. Xia, L. Yu, X. Y. Yu and X. W. Lou, *Nat. Commun.*, 2015, **6**, 6512.
2 B. Y. Xia, Y. Yan, N. Li, H. B. Wu, X. W. Lou and X. Wang, *Nat. Energy*, 2016, **1**, 15006.
3 F. X. Ma, H. B. Wu, B. Y. Xia, C. Y. Xu and X. W. Lou, *Angew. Chem., Int. Ed.*, 2015, **54**, 15395–15399.
4 L. Han, X. Y. Yu and X. W. Lou, *Adv. Mater.*, 2016, **28**, 4601–4605.
5 Y. Lee, J. Suntivich, K. J. May, E. E. Perry and Y. Shao-Horn, *J. Phys. Chem. Lett.*, 2012, **3**, 399–404.
6 J. Suntivich, K. J. May, H. A. Gasteiger, J. B. Goodenough and Y. Shao-Horn, *Science*, 2011, **334**, 1383–1385.
7 Q. Yu, X. G. Meng, T. Wang, P. Li, L. Q. Liu, K. Chang, G. G. Liu and J. H. Ye, *Chem. Commun.*, 2015, **51**, 3630–3633.
8 Y. Matsumoto, S. Yamada, T. Nishida and E. Sato, *J. Electrochem. Soc.*, 1980, **127**, 2360–2364.
9 F. Cheng, T. Zhang, Y. Zhang, J. Du, X. Han and J. Chen, *Angew. Chem., Int. Ed.*, 2013, **52**, 2474–2477.
10 X. Zhao, J. Feng, S. Chen, Y. Huang, T. C. Sum and Z. Chen, *Phys. Chem. Chem. Phys.*, 2017, **19**, 1074–1082.
11 T. Yamashita and P. Hayes, *Appl. Surf. Sci.*, 2008, **254**, 2441–2449.
12 K. Ueda, Y. Muraoka, H. Tabata and T. Kawai, *Appl. Phys. Lett.*, 2001, **78**, 512.

13 Y. Zhang, X. Wang, Y. Zhu, B. Hou, X. Yang, X. Liu, J. Wang, J. Li and T. Zhang, *J. Phys. Chem. C*, 2014, **118**, 1999–2010.
14 B. T. Flynn, K. H. Zhang, V. Shutthanandan, T. Varga, R. J. Colby, R. P. Oleksak, S. Manandhar, M. H. Engelhard, S. A. Chambers and M. A. Henderson, *Appl. Surf. Sci.*, 2015, **330**, 309–315.
15 (*a*) A. Nenning, A. K. Opitz, C. Rameshan, R. Rameshan, R. Blume, M. Hävecker, A. Knop-Gericke, G. N. Rupprechter, B. Klötzer and J. R. Fleig, *J. Phys. Chem. C*, 2016, **120**, 1461–1471; (*b*) A. Braun, J. Richter, A. Harvey, A. Infortuna, A. Frei, E. Pomjakushina, B. S. Mun, P. Holtappels, U. Vogt and K. Conder, 2011, arXiv preprint, arXiv: 1106.1014.
16 A. K. Opitz, A. Nenning, C. Rameshan, R. Rameshan, R. Blume, M. Hävecker, A. Knop-Gericke, G. Rupprechter, J. Fleig and B. Klötzer, *Angew. Chem., Int. Ed.*, 2015, **54**, 2628–2632.
17 (*a*) A. Chainani, M. Mathew and D. Sarma, *Phys. Rev. B: Condens. Matter Mater. Phys.*, 1993, **48**, 14818; (*b*) Y. Nohara, S. Yamamoto and T. Fujiwara, *Phys. Rev. B: Condens. Matter Mater. Phys.*, 2009, **79**, 195110.
18 J. B. Goodenough, *Phys. Rev.*, 1955, **100**, 564.
19 C. Zener, *Phys. Rev.*, 1951, **82**, 403.
20 S. Y. Smolin, M. D. Scafetta, A. K. Choquette, M. Y. Sfeir, J. B. Baxte and S. J. May, *Chem. Mater.*, 2015, **28**, 97–105.
21 N. Afifah and R. Saleh, *J. Phys.: Conf. Ser.*, 2016, **710**, 012030.
22 R. A. Eichel, *Phys. Chem. Chem. Phys.*, 2011, **13**, 368–384.
23 Y. Wang, J. Zhu, L. Zhang, X. Yang, L. Lu and X. Wang, *Mater. Lett.*, 2006, **60**, 1767–1770.
24 (*a*) S. Hull, S. T. Norberg, I. Ahmed, S. G. Eriksson, D. Marrocchelli and P. Madden, *J. Solid State Chem.*, 2009, **182**, 2815–2821; (*b*) Y.-M. Kim, J. He, M. D. Biegalski, H. Ambaye, V. Lauter, H. M. Christen, S. T. Pantelides, S. J. Pennycook, S. V. Kalinin and A. Y. Borisevich, *Nat. Mater.*, 2012, **11**, 888–894.
25 D. Neagu, G. Tsekouras, D. N. Miller, H. Ménard and J. T. Irvine, *Nat. Chem.*, 2013, **5**, 916–923.
26 Y. Chen, Z. Cai, Y. Kuru, W. Ma, H. L. Tuller and B. Yildiz, *Adv. Energy Mater.*, 2013, **3**, 1221–1229.

